A see-saw variability in tropical cyclone genesis between the western North Pacific and the North Atlantic shaped by Atlantic multidecadal variability

Chao Wang[1,2], Bin Wang[2,3], Liguang Wu[4] and Jing-Jia Luo[1]

[1]Key Laboratory of Meteorological Disaster of Ministry of Education, Nanjing University of Information Science and Technology, Nanjing, 210044, China

[2]Earth System Modeling Center, Nanjing University of Information Science and Technology, Nanjing, 210044, China

[3]Department of Atmospheric Sciences and International Pacific Research Center, University of Hawaii at Manoa, Honolulu, Hawaii, 96822, USA

[4]Department of Atmospheric and Oceanic Sciences and Institute of Atmospheric Sciences, Fudan University, Shanghai, 200438, China

Revised for *Journal of Climate*

Janurary 7, 2022

Corresponding author: Chao Wang and Bin Wang

E-mail address: wangchao@nuist.edu.cn; wangbin@hawaii.edu

Early Online Release: This preliminary version has been accepted for publication in *Journal of Climate* be fully cited, and has been assigned DOI 10.1175/JCLI-D-21-0529.1. The final typeset copyedited article will replace the EOR at the above DOI when it is published.

Abstract

Variabilities in tropical cyclone (TC) activity are commonly interpreted in individual TC basins. We identify an anti-phase decadal variation in TC genesis between the western North Pacific (WNP) and North Atlantic (NA). An inactive (active) WNP TC genesis concurs with an enhanced (suppressed) NA TC genesis. We propose that the trans-basin TC connection results from a subtropical east-west 'relay' teleconnection triggered by Atlantic multidecadal oscillation (AMO), involving a chain atmosphere-ocean interaction in the North Pacific. During a negative AMO phase, the tropical NA cooling suppresses local convective heating that further stimulates a descending low-level anti-cyclonic circulation in the tropical NA and eastern North Pacific as a Rossby wave response, inhibiting the NA TC genesis. Meanwhile, the anomalous southwesterly to the western flank of the anomalous anti-cyclonic circulation tends to weaken the surface evaporation and warm the SST over the subtropical eastern North Pacific (southwest-northeast oriented zone from the tropical central Pacific to the subtropical west coast of North America). The SST warming further sustains a cyclonic circulation anomaly over the WNP by local atmosphere-ocean interaction and the Bjerknes feedback, promoting the WNP TC genesis. This trans-basin linkage helps us interpret the moderate amplitude of variations in TC genesis frequency in the Northern Hemisphere.

Accepted for publication in *Journal of Climate*. DOI 10.1175/JCLI-D-21-0529.1.

1. Introduction

Tropical cyclones (TCs) account for most natural catastrophic losses in the world, mainly affecting islands and coastal regions (Pielke and Landsea 1998; Pielke et al. 2008; Zhang et al. 2009; Peduzzi et al. 2012). It is thus of great interest to understand the variability of TC activity both scientifically and socially. However, whether induced by natural or anthropogenic forcing, climate variability in TC activity has been commonly investigated in individual TC basins. For instance, in the North Atlantic (NA), the recent active TC activity has been attributed to several factors, including global warming (Emanuel 2005; Elsner et al. 2008; Holland and Webster 2007), Atlantic Multidecadal Oscillation (AMO) (Goldenberg et al. 2001), and the Atlantic Meridional Mode (AMM) (Vimont and Kossin 2007; Kossin and Vimont 2007), or a combination of global warming and AMO (Wang and Wu 2013). For the western North Pacific (WNP) basin, TC activity experiences an unprecedented inactive period in the recent two decades (Liu and Chan 2013; Wu et al. 2015; Zhao et al. 2018), which is thought to be related to a negative phase of Pacific Decadal Oscillation (PDO) (Liu and Chan 2013; He et al. 2015; Hong et al. 2016), remote forcing from the Atlantic (Yu et al. 2016; Zhang et al. 2018), and the aerosol forcing (Takahashi et al. 2017).

The linkage of the TC activity in the NA and that in the adjacent eastern North Pacific (ENP) has been noticed. For example, a see-saw relationship has been found in TC activity in the NA and the eastern North Pacific(Elsner and Kara 1999), which results from the oppositely varied large-scale conditions in the two basins that are

Accepted for publication in *Journal of Climate.* DOI 10.1175/JCLI-D-21-0529.1.

induced by El Niño–Southern Oscillation (ENSO), AMO, and/or AMM (Frank and Young 2007; Wang and Lee 2009; Patricola et al. 2017). Wang et al (2020) found that the anti-varied large-scale condtions in the NA and the North Pacific are linked to the anticorrelated stationary wave activitives (tropical upper-tropospheric troughs) in the two basins.

Recent studies found the climate variabilities in the Pacific and Atlantic oceans are connected through atmosphere-ocean interactions (McGregor et al. 2014; Li et al. 2015b; Sun et al. 2017; Cai et al. 2019; Wang 2019; Yang et al. 2020; Meehl et al. 2021), which implies a possible linkage between the large-scale conditions in the Pacific and the Atlantic and thus between the TC activities in the two basins. However, up to now, the connection between the TC genesis in the WNP and the NA has not yet been documented. The present study investigates the relationship between the TC geneses in the two basins. As the two major basins of the Northern Hemisphere (NH) TC activity, exploring their intrinsic connection is helpful to understand variations in TC activity from a hemisphere framework. We found a see-saw relationship between TC geneses in the NA and WNP on the decadal timescale. We then interpret this linkage in terms of planetary circulation variability and the causality revealed by coupled model experiments. The finding here provides additional evidence for interpreting the moderate magnitude of variation in TC genesis number in the NH.

2. Materials and methods

TC genesis frequencies in the NA and ENP were derived from the Revised

Accepted for publication in *Journal of Climate.* DOI 10.1175/JCLI-D-21-0529.1.

Hurricane Database (HURDAT2) of the National Hurricane Center (NHC) (Landsea et al. 2010; Landsea and Franklin 2013). For the WNP, we used the three best track datasets compiled by the Joint Typhoon Warning Center (JTWC), the Regional Specialized Meteorological Center of Japan Meteorological Agency (JMA), and the Shanghai Typhoon Institute of China Meteorological Administration (CMA, Ying et al. 2014). The arithmetic mean of the three datasets was used to reduce the possible uncertainty among different datasets in the WNP. While the archived intensity records in the three best track data have discrepancies, the TC genesis frequencies are generally consistent with each other even back to the pre-satellite era (Wu et al. 2006; Kossin et al. 2007; Song et al. 2010). Since the maximum wind speed data are only available since 1977 in the JMA best track, we converted the intensity estimated by the TC center pressure before 1977 following the wind-pressure relationship proposed by Atkinson and Holliday (1977). TCs are defined as those in the dataset whose maximum wind speed reaches tropical storm intensity (17.2 m s^{-1}). The beginning years of the TC records in JTWC, CMA, and JMA best track datasets are 1945, 1949, and 1951, respectively. Therefore, our analysis period covers 1951-2018. The results generally resemble those with the relatively reliable TC data since 1960 (Chan 2006). The reason for using 1951 as the start year is that we want to use as long as possible available data to study the decadal variation. In addition, the monthly mean wind data from the fifth-generation atmospheric reanalysis of the European Centre for Medium-Range Weather Forecasts (ERA5) (Hersbach et al. 2020) were adopted to quantify the large-scale conditions. Monthly mean sea surface temperature (SST) from version 5

Accepted for publication in *Journal of Climate*. DOI 10.1175/JCLI-D-21-0529.1.

of the National Oceanic and Atmospheric Administration Extended Reconstructed SST (ERSST) dataset (Huang et al. 2017) was used.

Two empirical genesis indexes were used to demonstrate the combined influences of anomalous large-scale conditions on TC genesis. One is the dynamical genesis potential index (DGPI) proposed by Wang and Murakami (2020). The formulation of the GPI is as follows

$$DGPI = (2 + 0.1V_s)^{-1.7}\left(5.5 - \frac{\partial u}{\partial y}10^5\right)^{2.3}(5 - 20\omega)^{3.3}(5.5 + |10^5\eta|)^{2.4}e^{-11.8} - 1$$

Where V_s is the magnitude of the vertical wind shear (m s^{-1}) between 850 and 200 hPa, $\frac{\partial u}{\partial y}$ is the meridional gradient of zonal wind (s^{-1}) at 500 hPa, ω is the 500 hPa vertical pressure velocity (Pa s^{-1}) and η is the absolute vorticity (s^{-1}) at 850 hPa. The second is the genesis potential index (GPI) proposed by Emanuel and Nolan (2000), which is defined as

$$\text{GPI} = |10^5\eta|^{\frac{3}{2}}\left(\frac{\mathcal{H}}{50}\right)^3\left(\frac{Vp}{50}\right)^3(1 + 0.1Vshear)^{-2}$$

where η is the absolute vorticity at 850 hPa (s^{-1}), $\mathcal{H}$ is the relative humidity at 600 hPa (%), Vp is the maximum potential intensity (MPI, m s^{-1}), and Vshear is the magnitude of the vertical wind shear between 850 hPa and 200 hPa (m s^{-1}).

A five-year running mean was first applied to all observational data to focus on the decadal variability. Statistical significance of regression and correlation analyses was assessed using the two-tailed Student's t-test (Wilks 2006). Because the running mean tends to decrease the degree of freedom, the effective degree of freedom was used to estimate the significance of correlation and regression coefficients based on the running mean variables (Davis 1976). We conducted two

Accepted for publication in *Journal of Climate*. DOI 10.1175/JCLI-D-21-0529.1.

numerical experiments with a coupled climate model (Cao et al. 2015, 2017) to illustrate the impacts of AMO on large-scale circulations in the WNP. The atmospheric component of the coupled model is ECHAM version 5.3 atmospheric global climate model (Roeckner et al. 2003) with a horizontal resolution of spectral triangular 42 and 31 levels in vertical. The Nucleus for European Modeling of the Ocean (Madec 2008) with a 2°*2° horizontal resolution and 31 vertical levels is applied as the oceanic component model, while the sea ice component model is version 4.1 of the Los Alamos Sea Ice Model. The coupled mode shows reasonable skill in reproducing the annual cycle, monsoon variability, and ENSO (Cao et al. 2015). The model configuration is the same as that was described in Wang et al. (2018). One is a control run which is a freely coupled run with external forcings (solar, volcanic, and greenhouse gases) fixed at 1990 conditions. The other is a partially coupled run, in which the reversed AMO-regressed SST anomalies were nudged to SST values in the NA (0°-50°N, 80°W-0°). Outside the North Atlantic, the model is fully coupled. Each experiment includes 40 ensemble members. The difference between the ensemble means of these two experiments was regarded as the responses to the AMO-related SST anomalies.

3 Result

3.1 A see-saw relationship in the TC genesis between the NA and WNP

TC genesis frequency experiences notable inter-decadal variations in both the WNP and the NA (Fig.1). In the WNP, three low-TC frequency periods (1951-

Accepted for publication in *Journal of Climate.* DOI 10.1175/JCLI-D-21-0529.1.

1960,1973–1985 and 1995-2018) and two high-TC frequency periods (1961–1972 and 1986–1994) can be identified, which is consistent with previous studies (Yumoto and Matsuura 2001; Liu and Chan 2013). Meanwhile, the NA TC genesis frequency is below normal during 1961-1994, but experiences two high-TC frequency periods (1951-1960 and 1995-2018) (Goldenberg et al. 2001; Emanuel 2005; Holland and Webster 2007). Interestingly, decadal fluctuations of the TC genesis frequency in the two basins are anti-correlated with a correlation coefficient of -0.62 ($p<0.01$) during 1951-2018. The correlation is still robust when their long-term trends are removed. The significant correlation is valid even though only one of the three best track datasets (CMA, JMA, and JTWC) was used to derive the WNP TC genesis frequency. Particularly, the correlation coefficients between the TC genesis frequency in the NA and the TC numbers derived from the CMA, JMA, and JTWC are -0.68, -0.52, and -0.49, respectively, which are significant at a 95% confidence level with the effective degrees of freedom. Moreover, the significant correlation (r=-0.47) still exists when only the peak season (July-October) of NA and WNP TC genesis was considered, while correlation in inactive season (season exclude peak season) is relatively low (r=-0.13).

We further examined the spatial distribution of the TC genesis anomalies to find the major decadal variability region (MVR) of this trans-basin linkage (Fig. 2). The WNP MVR is located mainly in the South China Sea, Philippine Sea (7.5°N-20°N, 120°E-155°E), and the region further east (7.5°N-30°N, 155°E-170°E). The NA MVR is found in the Gulf of Mexico (10°N-30°N, 100°W-80°W) and the Major

Accepted for publication in *Journal of Climate*. DOI 10.1175/JCLI-D-21-0529.1.

Development Zone (10°N-25°N, 80°W-20°W). The above decadal MVRs are slightly different from the main development regions determined by the interannual variability. On the decadal time scale, the annual TC genesis frequencies in the WNP MVR and the NA MVR are significantly correlated with a correlation coefficient of -0.53 during 1951-2018, suggesting that TC geneses in the two basins, although separated by thousands of miles, vary in tandem.

3.2 Large-scale circulation variations responsible for TC frequency changes

To understand the anti-correlation of the TC genesis between the NA and the WNP, we examined inter-decadal variations of the environmental conditions that might have profound impacts on TC genesis (Gray 1968; Hsieh et al. 2020). Here, we examined the anomalies in vertical wind shear (defined as the magnitude of the vector difference between zonal winds at 850 hPa and 200 hPa), 850 hPa relative vorticity, and 500hPa vertical motion associated with the decadal see-saw variation of the TC genesis frequencies in the two basins.

Figure 3 shows the July-October mean large-scale environment anomalies associated with the annual TC genesis frequency in the WNP. The decreased vertical wind shear to the east of 150°E and increased 850 hPa relative vorticity in the WNP MVR concur with the corresponding opposite changes of vertical wind shear and relative vorticity in the NA MVR (Figs. 3a-b). The strengthened vertical wind shear and weakened low-level vorticity in the NA MVR tend to suppress the TC genesis in the NA, while the weakened vertical wind shear and the enhanced low-level vorticity

Accepted for publication in *Journal of Climate.* DOI 10.1175/JCLI-D-21-0529.1.

over the WNP MVR favor the TC genesis in the WNP. The decreased vertical wind shear in the eastern MVR in the WNP is consistent with the inactive eastern WNP TC genesis in the recent decades (Liu and Chan 2013; Wu et al. 2015; Zhao et al. 2018). In terms of vertical motion, positive anomalies (descending motion) in the NA MVR, which tend to suppress the TC genesis in the NA, are concurrent with negative anomalies (ascending motion) in tropical central Pacific (Fig. 3c). The anomalous ascending motions in the eastern WNP MVR are conducive to a local TC genesis.

To estimate the overall influences of these large-scale condition anomalies on TC genesis, Fig. 3d shows empirical genesis index anomalies associated with the annual TC genesis frequency in the WNP. However, DGPI or GPI alone cannot describe decadal variabilities of TC genesis in the WNP and NA. Particularly, DGPI shows superior skill in describing decadal variability of WNP TC genesis (R=0.6) but poor skill representing in that of NA TC genesis (R=0.06), while GPI shows superior skill in describing decadal variability of NA TC genesis (R=0.82) but poor skill representing in that of WNP TC genesis (R=-0.43). The basin depended skill of empirical genesis index suggests that dominant factors controlling decadal variability of TC genesis for each basin may different (Fu et al. 2012; Peng et al. 2012). Therefore, we combined DGPI over the WNP and GPI over the NA to represent large-scale impacts on TC genesis (Fig. 3d). There are positive DGPI anomalies in the WNP MVR but negative GPI anomalies in the NA, which suggests that the overall influence of large-scale conditions can result in the seesaw variability in TC genesis. The coherence in the opposite variations in TC genesis and large-scale conditions indicates

Accepted for publication in *Journal of Climate.* DOI 10.1175/JCLI-D-21-0529.1.

that changes in large-scale environments are responsible for this see-saw relationship in the NA and the WNP TC geneses.

3.3 Causes of the opposite large-scale circulations between the WNP and NA

What mechanism drives the opposite variations in the large-scale condition in the NA and WNP? We noticed that both the TC genesis frequencies in the WNP and NA are significantly correlated with July-October mean AMO index (Schlesinger and Ramankutty 1994) with a correlation coefficient of -0.60 and 0.85, respectively, over 1951-2018 (Fig. 1). Thus, we hypothesize that the AMO is the main driver for this trans-basin linkage in large-scale conditions. The reasons follow.

Figure 4 shows the July-October mean relative SST and 850 hPa wind anomalies associated with the sign-reversed five-year running July-October mean AMO index during 1951-2018. Although some discrepancies exist in the tropical central Pacific, the AMO-related SST (Fig. 4a) displays a similar pattern to that of SST shown in Figure 3c. Note that the spatial distribution of SST anomaly or the relative SST to the tropical mean, not the local SST anomaly, determines the distribution of vertical motions (Vecchi and Soden 2007; Johnson and Xie 2010). Thus, the relative SST cooling in the tropical NA tends to generate anomalous descending motion in the NA MVR (Fig. 4b). Meanwhile, the associated suppressed convective heating can emanate an anti-cyclonic circulation over the tropical NA, acting to increase vertical wind shear and decrease low-level vorticity in the NA MVR (Fig. 4b). The enhanced descending motion, strengthened vertical wind shear and the

Accepted for publication in *Journal of Climate.* DOI 10.1175/JCLI-D-21-0529.1.

decreased low-level vorticity suppress NA TC genesis. In the North Pacific, the AMO-related SST features a prominent relative SST cooling in the mid-latitude North Pacific and the subtropical western Pacific but relative warming over the subtropical eastern North Pacific from Hawaii to Baja California and the tropical central Pacific. The relative SST warming in the elongated, southwest-northeast oriented zone from the tropical central Pacific to the subtropical west coast of North America is coupled to the cyclonic circulation extending from the tropical WNP to the subtropical eastern North Pacific through atmosphere-ocean interaction (Fig. 4b, Wang et al. 2000, 2003). Meanwhile, the tropical westerly anomalies are amplified and eventually drive an El Nino–like SST anomaly (Fig. 4a) through the Pacific Bjerknes feedback (Bjerknes 1969). The anomalous westerly winds tend to shift the low-level monsoon trough and the upper-level tropical upper tropospheric trough eastward (Wang and Wu 2016), boosting the WNP TC genesis by increasing low-level vorticity in the WNP MVR (Figs. 3a-b). The similarity between the regressed SST and wind patterns against the AMO and the WNP TC genesis frequency (Fig. 3c and Figs. 4a-b) suggests an association of the AMO and TC genesis over the WNP. Moreover, the empirical genesis index anomalies associated with AMO show positive DGPI anomalies in the WNP but negative GPI anomalies in the NA (Fig. 4c), suggesting the key role of AMO in the opposite large-scale condition anomalies in the WNP and NA. To examine the contributions of each large-scale parameter, we calculated the empirical genesis index by varying each component with other variables fixed at their long-term climatological values (Figs. 4d-e). The maximum potential intensity, mid-level

Accepted for publication in *Journal of Climate.* DOI 10.1175/JCLI-D-21-0529.1.

humidity, and vertical wind shear largely contribute to the negative GPI anomalies in the NA (Fig. 4e), while the positive DGPI anomalies in the WNP are mainly contributed by vertical wind shear, low-level vorticity, and meridional gradient of mid-level zonal wind (Fig. 4d). The diagnostic suggests that AMO tends to modulate local maximum potential intensity, mid-level humidity and vertical wind shear in the NA, and remotely generates a cyclonic/anti-cyclonic circulation over the WNP that affects large-scale conditions such as vorticity and vertical wind shear.

A remaining issue is how the AMO remotely modulates the large-scale circulations over the WNP? Here we suggest that the NA cooling and the WNP cyclonic anomalies are linked by an east-west 'relay' teleconnection mechanism that involves a chain atmosphere-ocean interaction in the NP. First, during a negative AMO phase, the NA cooling suppresses tropical NA convective heating, resulting in a descending low-level anti-cyclonic circulation to its west as a Rossby wave response in the eastern North Pacific. The anomalous southwesterly to the western flank of the anomalous anti-cyclone tends to weaken the trade wind speed and surface evaporation, and increase SST over the southwest-northeast oriented zone from the tropical central Pacific to the subtropical west coast of North America (Figs. 4a-b). The resultant warming can further induce a cyclonic circulation anomaly over the WNP. The North Pacific SST and WNP circulation anomalies can be viewed as a relay response to the NA cooling. The local atmosphere-ocean feedback plays an essential role in the relay mechanism. The local atmosphere-ocean feedback also plays an essential role in sustaining the WNP cyclonic anomalies (Wang et al. 2000; Lau and Nath 2003; Wang

Accepted for publication in *Journal of Climate.* DOI 10.1175/JCLI-D-21-0529.1.

et al. 2013). On the one hand, the central North Pacific warming increases precipitation heating, enhancing the WNP cyclonic anomalies by exciting westward-propagating ascending Rossby waves. On the other hand, the cyclonic anomalies-induced southwesterly anomalies reduce evaporation cooling by weakening trade wind speed and further warm the central-eastern North Pacific (Fig. 4). Moreover, the tropical westerlies can facilitate a weakened zonal SST gradient, which further intensifies the westerlies and ultimately rises an El Nino-like SST anomaly in the Pacific through the Bjerknes feedback (Bjerknes 1969). The two positive feedbacks can maintain both the central-eastern NP warming and the WNP low-level cyclonic vorticity anomalies.

We performed numerical experiments (section 2) to verify the east-west relay teleconnection mechanism. Although there are some discrepancies in the simulated SST and large-scale circulations that may result from bias in exchange efficiency of heat flux between atmosphere and ocean associated with the simulated mean trade wind strength (Czaja et al. 2002; Yu et al. 2015) and external forcings (Meehl et al. 2021), the numerical experiments generally reproduced the observed SST and 850hPa circulation patterns in the NH (Figs. 4 and 5). With the AMO-related SST cooling in the NA (Fig. 5a), the suppressed convective heating stimulates an anti-cyclonic circulation across the NA and the eastern North Pacific as a Rossby wave response (Fig. 5b). Meanwhile, the anomalous southwesterly to the western flank of the anomalous anti-cyclonic circulation reduces the trade winds and surface latent heat loss, thereby warm the central North Pacific in the southwest-northeast tilted region.

Accepted for publication in *Journal of Climate*. DOI 10.1175/JCLI-D-21-0529.1.

The central North Pacific warming can then enhance local precipitation and further induce the low-level cyclonic anomalies over the WNP MVR as a Rossby wave response (Figs. 5a-b). Meanwhile, tropical westerlies associated with the cyclonic circulation can further interact with the Pacific Ocean, intensifying the winds and ultimately rising an El Nino-like SST anomaly in the Pacific Ocean (Fig. 5a). The large-scale parameters associated with the cyclonic anomalies such as weakened vertical wind shear and strengthened low-level vorticity are favorable for TC genesis in the WNP. Accordingly, there are positive DGPI anomalies in the WNP but negative GPI anomalies in the NA, indicating the opposite impact of AMO-driven large-scale condition on TC genesis in the NA and WNP (Fig. 5c). Generally, the results support the proposed AMO-related east-west relay teleconnection mechanism of the trans-basin linkage in large-scale circulation and the opposite impact of AMO-driven large-scale condition in the WNP an NA. Therefore, we conclude the AMO acts as a key pacemaker for large-scale conditions in the WNP, and thus for the trans-basin linkage in TC genesis between the WNP and the NA.

4. Conclusion, discussion, and implication

Variabilities in TC activity are commonly interpreted in individual TC basins, while trans-basin linkage in TC activity between the WNP and NA remains elusive. We find an inactive (active) WNP TC genesis concurs with an enhanced (suppressed) NA TC genesis. This trans-basin linkage is consistent with the opposing large-scale condition anomalies in the two basins. We propose that the trans-basin connection in

Accepted for publication in *Journal of Climate.* DOI 10.1175/JCLI-D-21-0529.1.

TC genesis results from the AMO-initiated east-west 'relay' teleconnection mechanism that involves a chain atmosphere-ocean interaction in the North Pacific. During a negative AMO phase, the NA cooling suppresses convective heating and stimulates a descending low-level anti-cyclonic circulation to its west as a Rossby wave response in the NA and eastern North Pacific, inhibiting the NA TC genesis. Meanwhile, the anomalous southwesterly to the western flank of the anomalous anti-cyclonic circulation tends to weaken the surface evaporation and thus warm to the SST over the southwest-northeast oriented zone from the tropical central Pacific to the subtropical west coast of North America. The SST warming further sustains a cyclonic circulation anomaly over the WNP by local atmosphere-ocean interaction and the Pacific Bjerknes feedback, promoting TC genesis in the WNP.

Since previous studies have shown that PDO can lead to notable variations in TC activity in the WNP and NA (Li et al. 2015a; Zhao et al. 2020), one may query about its possible contribution to the seesaw variability in TC genesis. Statistically, PDO index does positively correlated with TC genesis frequency in the WNP ($r=0.36$, $p=0.08$) and negatively correlated with TC genesis frequency in the NA ($r=-0.59$, $p<0.01$). The opposite sign of correlations between TC genesis frequency, AMO and PDO suggest that the seesaw variability of TC genesis is collectively contributed by an opposite phase of AMO and PDO. Particularly, the seesaw variability is prominent during the period when phases of PDO and AMO are opposite (1951-1962, 1977-1998 and 1999-2018), while the seesaw variability is weak during 1963-1976 when both AMO and PDO experience negative phase (Fig. 1). Although there is no significant

Accepted for publication in *Journal of Climate*. DOI 10.1175/JCLI-D-21-0529.1.

simultaneous correlation (r=-0.24) between the AMO and PDO, evolutions of PDO and AMO are sequentially interactive (Wu et al. 2011; Li et al. 2015b; Meehl et al. 2021). Particularly, the AMO-related SST can initiate an opposite-sign SST response in the tropical Pacific, resulting in anti-phases of AMO and PDO during periods such as 1951-1962, 1977-1998 and 1999-2018 (Fig. 1). However, the PDO-related SST can initiate a same-sign SST response in the tropical Atlantic, leading to in-phase of AMO and PDO such as 1963-1976 (Fig. 1, Li et al. 2015b; Meehl et al. 2021). Our numerical experiment also confirmed that AMO can drive an opposite phase of PDO (Fig. 5). The results suggest that the opposite-sign SST in the tropical Atlantic and tropical Pacific or the opposite phase of AMO and PDO is mainly driven by AMO, eventually resulting in the seesaw variability of TC genesis. While PDO tends to generate a same-sign SST response in the NA or an in-phase of AMO and PDO (Meehl et al. 2021), which may weaken the seesaw variability of TC genesis. The results suggest that AMO may play a dominant role in the seesaw variability of TC genesis. One may note the correlation between TC genesis frequency in the peak season in the two basins is slightly weaker than the coreesponding correlation with annual TC genesis frequency (section 3), which may be associated with the delayed oceanic response of Pacific SST to the AMO forcing (Li et al. 2015b; Yang et al. 2020).

The opposite variation in TC genesis in the NA and the WNP has important implications for interpreting the moderate year-to-year variations in TC genesis frequency in the NH. Considering nearly 70% of TCs in the NH are formed in these

Accepted for publication in *Journal of Climate*. DOI 10.1175/JCLI-D-21-0529.1.

two basins, the anti-varied TC genesis frequencies in the WNP and the NA can contribute to the moderate variations in TC genesis frequency in the NH on the decadal time scale. Such a trans-basin linkage may shed light on the projected suppressed TC genesis in the WNP but enhanced TC genesis in the NA in global warming scenarios (Li et al. 2010; Villarini et al. 2011; Murakami et al. 2020).

In 2020, the Atlantic basin experienced the busiest hurricane season, but typhoon activity over the WNP was below normal. However, how the proposed decadal linkage contributed to the extreme TC season in 2020 and how this linkage is reproduced in the current state-of-art climate models deserve further explorations.

Acknowledgments

This study was jointly supported by the National Natural Science Foundation of China (Grant No. 42088101, 42075031, 41420104002, 41730961 and 41922033). It is the Earth System Modeling Center publication XXX at the Nanjing University of Information Science and Technology, the School of Ocean and Earth Science and Technology (SOEST) publication number XXXX, and the IPRC publication number YYYY. Tropical cyclone data of CMA, JMA, JTWC and NHC can be requested at http://tcdata.typhoon.org.cn/en/zjljsjj_zlhq.html, http://www.jma.go.jp/jma/jma-eng/jma-center/rsmc-hp-pub-eg/besttrack.html and https://www.metoc.navy.mil/jtwc/jtwc.html?western-pacific, respectively. environmental variables were obtained from https://www.ecmwf.int/en/forecasts/datasets/reanalysis-datasets/era5, and SST was

Accepted for publication in *Journal of Climate.* DOI 10.1175/JCLI-D-21-0529.1.

download at https://psl.noaa.gov/data/gridded/data.noaa.ersst.v5.html. The AMO index was download at https://psl.noaa.gov/data/timeseries/AMO/.

References:

Atkinson, G. D., and C. R. Holliday, 1977: Tropical Cyclone Minimum Sea Level Pressure/Maximum Sustained Wind Relationship for the Western North Pacific. *Mon. Weather Rev.*, **105**, 421–427, https://doi.org/10.1175/1520-0493(1977)105<0421:TCMSLP>2.0.CO;2.

Bjerknes, J., 1969: Atmospheric teleconnections from the equatorial pacific. *Mon. Weather Rev.*, **97**, 163–172, https://doi.org/doi.org/10.1175/1520-0493.

Cai, W., and Coauthors, 2019: Pantropical climate interactions. *Science (80-.).*, **363**, eaav4236, https://doi.org/10.1126/science.aav4236.

Cao, J., B. Wang, B. Xiang, J. Li, T. Wu, X. Fu, L. Wu, and J. Min, 2015: Major modes of short-term climate variability in the newly developed NUIST Earth System Model (NESM). *Adv. Atmos. Sci.*, **32**, 585–600, https://doi.org/10.1007/s00376-014-4200-6.

——, and Coauthors, 2017: The NUIST Earth System Model (NESM) version 3: Description and preliminary evaluation. *Geosci. Model Dev. Discuss.*, 1–53, https://doi.org/10.5194/gmd-2017-206.

Chan, J. C., 2006: Comment on "Changes in tropical cyclone number, duration, and intensity in a warming environment." *Science (80-.).*, **311**, 1713; author reply

Accepted for publication in *Journal of Climate.* DOI 10.1175/JCLI-D-21-0529.1.

1713, https://doi.org/10.1126/science.1121522.

Czaja, A., P. van der Vaart, and J. Marshall, 2002: A Diagnostic Study of the Role of Remote Forcing in Tropical Atlantic Variability. *J. Clim.*, **15**, 3280–3290, https://doi.org/10.1175/1520-0442(2002)015<3280:ADSOTR>2.0.CO;2.

Davis, R. E., 1976: Predictability of Sea Surface Temperature and Sea Level Pressure Anomalies over the North Pacific Ocean. *J. Phys. Oceanogr.*, **6**, 249–266, https://doi.org/10.1175/1520-0485(1976)006<0249:possta>2.0.co;2.

Elsner, J. B., and A. B. Kara, 1999: *Hurricanes of the North Atlantic : Climate and Society: Climate and Society*. 693 pp.

Elsner, J. B., J. P. Kossin, and T. H. Jagger, 2008: The increasing intensity of the strongest tropical cyclones. *Nature*, **455**, 92–95, https://doi.org/10.1038/nature07234.

Emanuel, K., 2005: Increasing destructiveness of tropical cyclones over the past 30 years. *Nature*, **436**, 686–688, https://doi.org/10.1038/nature03906.

Frank, W. M., and G. S. Young, 2007: The Interannual Variability of Tropical Cyclones. *Mon. Weather Rev.*, **135**, 3587–3598, https://doi.org/10.1175/mwr3435.1.

Fu, B., M. S. Peng, T. Li, and D. E. Stevens, 2012: Developing versus Nondeveloping Disturbances for Tropical Cyclone Formation. Part II: Western North Pacific*. *Mon. Weather Rev.*, **140**, 1067–1080, https://doi.org/10.1175/2011mwr3618.1.

Goldenberg, S. B., C. W. Landsea, A. M. Mestas-Nuñez, W. M. Gray, A. M. Mestas-Nunez, and W. M. Gray, 2001: The recent increase in Atlantic hurricane activity:

Accepted for publication in *Journal of Climate.* DOI 10.1175/JCLI-D-21-0529.1.

Causes and implications. *Science (80-.).*, **293**, 474–479, https://doi.org/10.1126/science.1060040.

Gray, W. M., 1968: Global view of the origin of tropical disturbances and storms. *Mon. Weather Rev.*, **96**, 669–700.

He, H., J. Yang, D. Gong, R. Mao, Y. Wang, and M. Gao, 2015: Decadal changes in tropical cyclone activity over the western North Pacific in the late 1990s. *Clim. Dyn.*, https://doi.org/10.1007/s00382-015-2541-1.

Hersbach, H., and Coauthors, 2020: The ERA5 global reanalysis. *Q. J. R. Meteorol. Soc.*, **146**, 1999–2049, https://doi.org/10.1002/qj.3803.

Holland, G. J., and P. J. Webster, 2007: Heightened tropical cyclone activity in the North Atlantic: natural variability or climate trend? *Philos Trans A Math Phys Eng Sci*, **365**, 2695–2716, https://doi.org/10.1098/rsta.2007.2083.

Hong, C.-C., Y.-K. Wu, and T. Li, 2016: Influence of climate regime shift on the interdecadal change in tropical cyclone activity over the Pacific Basin during the middle to late 1990s. *Clim. Dyn.*, **47**, 2587–2600, https://doi.org/10.1007/s00382-016-2986-x.

Hsieh, T.-L., G. A. Vecchi, W. Yang, I. M. Held, and S. T. Garner, 2020: Large-scale control on the frequency of tropical cyclones and seeds: a consistent relationship across a hierarchy of global atmospheric models. *Clim. Dyn. 2020 5511*, **55**, 3177–3196, https://doi.org/10.1007/S00382-020-05446-5.

Huang, B., and Coauthors, 2017: Extended Reconstructed Sea Surface Temperature, Version 5 (ERSSTv5): Upgrades, Validations, and Intercomparisons. *J. Clim.*, **30**,

Accepted for publication in *Journal of Climate.* DOI 10.1175/JCLI-D-21-0529.1.

8179–8205, https://doi.org/10.1175/JCLI-D-16-0836.1.

Johnson, N. C., and S.-P. Xie, 2010: Changes in the sea surface temperature threshold for tropical convection. *Nat. Geosci.*, **3**, 842–845, https://doi.org/10.1038/ngeo1008.

Kossin, J. P., and D. J. Vimont, 2007: A more general framework for understanding atlantic hurricane variability and trends. *Bull. Am. Meteorol. Soc.*, **88**, 1767–1781, https://doi.org/10.1175/BAMS-88-11-1767.

Kossin, J. P., K. R. Knapp, D. J. Vimont, R. J. Murnane, and B. A. Harper, 2007: A globally consistent reanalysis of hurricane variability and trends. *Geophys. Res. Lett.*, **34**, https://doi.org/10.1029/2006gl028836.

Landsea, C. W., and J. L. Franklin, 2013: Atlantic Hurricane Database Uncertainty and Presentation of a New Database Format. *Mon. Weather Rev.*, **141**, 3576–3592, https://doi.org/10.1175/MWR-D-12-00254.1.

Landsea, C. W., G. A. Vecchi, L. Bengtsson, and T. R. Knutson, 2010: Impact of Duration Thresholds on Atlantic Tropical Cyclone Counts*. *J. Clim.*, **23**, 2508–2519.

Lau, N. C., and M. J. Nath, 2003: Atmosphere-ocean variations in the Indo-Pacific sector during ENSO episodes. *J. Clim.*, **16**, 3–20, https://doi.org/10.1175/1520-0442(2003)016<0003:AOVITI>2.0.CO;2.

Li, T., M. Kwon, M. Zhao, J.-S. Kug, J.-J. Luo, and W. Yu, 2010: Global warming shifts Pacific tropical cyclone location. *Geophys. Res. Lett.*, **37**, n/a-n/a, https://doi.org/10.1029/2010gl045124.

Accepted for publication in *Journal of Climate*. DOI 10.1175/JCLI-D-21-0529.1.

Li, W., L. Li, and Y. Deng, 2015a: Impact of the Interdecadal Pacific Oscillation on Tropical Cyclone Activity in the North Atlantic and Eastern North Pacific. *Sci. Rep.*, **5**, 1–8, https://doi.org/10.1038/srep12358.

Li, X., S.-P. Xie, S. T. Gille, and C. Yoo, 2015b: Atlantic-induced pan-tropical climate change over the past three decades. *Nat. Clim. Chang.*, **6**, 275–279, https://doi.org/10.1038/nclimate2840.

Liu, K. S., and J. C. L. Chan, 2013: Inactive period of Western North Pacific tropical cyclone activity in 1998-2011. *J. Clim.*, **26**, 2614–2630, https://doi.org/10.1175/JCLI-D-12-00053.1.

McGregor, S., A. Timmermann, M. F. Stuecker, M. H. England, M. Merrifield, F. F. Jin, and Y. Chikamoto, 2014: Recent walker circulation strengthening and pacific cooling amplified by atlantic warming. *Nat. Clim. Chang.*, **4**, 888–892, https://doi.org/10.1038/nclimate2330.

Meehl, G. A., and Coauthors, 2021: Atlantic and Pacific tropics connected by mutually interactive decadal-timescale processes. *Nat. Geosci.*, **14**, 36–42, https://doi.org/10.1038/s41561-020-00669-x.

Murakami, H., T. L. Delworth, W. F. Cooke, M. Zhao, B. Xiang, and P.-C. Hsu, 2020: Detected climatic change in global distribution of tropical cyclones. *Proc. Natl. Acad. Sci.*, 201922500, https://doi.org/10.1073/pnas.1922500117.

Patricola, C. M., R. Saravanan, and P. Chang, 2017: A teleconnection between Atlantic sea surface temperature and eastern and central North Pacific tropical cyclones. *Geophys. Res. Lett.*, **44**, 1167–1174,

Accepted for publication in *Journal of Climate*. DOI 10.1175/JCLI-D-21-0529.1.

https://doi.org/10.1002/2016GL071965.

Peduzzi, P., B. Chatenoux, H. Dao, A. De Bono, C. Herold, J. Kossin, F. Mouton, and O. Nordbeck, 2012: Global trends in tropical cyclone risk. *Nat. Clim. Chang.*, **2**, 289–294, https://doi.org/10.1038/nclimate1410.

Peng, M. S., B. Fu, T. Li, and D. E. Stevens, 2012: Developing versus Nondeveloping Disturbances for Tropical Cyclone Formation. Part I: North Atlantic*. *Mon. Weather Rev.*, **140**, 1047–1066, https://doi.org/10.1175/2011mwr3617.1.

Pielke, R. A., and C. W. Landsea, 1998: Normalized Hurricane Damages in the United States: 1925–95. *Weather Forecast.*, **13**, 621–631, https://doi.org/10.1175/1520-0434(1998)013<0621:NHDITU>2.0.CO;2.

——, J. Gratz, C. W. Landsea, D. Collins, M. A. Saunders, and R. Musulin, 2008: Normalized Hurricane Damage in the United States: 1900–2005. *Nat. Hazards Rev.*, **9**, 29–42, https://doi.org/10.1061/(ASCE)1527-6988(2008)9:1(29).

Roeckner, E., and Coauthors, 2003: The atmospheric general circulation model ECHAM 5. PART I: Model description.

Schlesinger, M. E., and N. Ramankutty, 1994: An oscillation in the global climate system of period 65–70 years. *Nature*, **367**, 723–726, https://doi.org/10.1038/367723a0.

Song, J.-J., Y. Wang, and L. Wu, 2010: Trend discrepancies among three best track data sets of western North Pacific tropical cyclones. *J. Geophys. Res.*, **115**, https://doi.org/10.1029/2009jd013058.

Sun, C., F. Kucharski, J. Li, F. F. Jin, I. S. Kang, and R. Ding, 2017: Western tropical

Accepted for publication in *Journal of Climate.* DOI 10.1175/JCLI-D-21-0529.1.

Pacific multidecadal variability forced by the Atlantic multidecadal oscillation. *Nat. Commun.*, **8**, 1–10, https://doi.org/10.1038/ncomms15998.

Takahashi, C., M. Watanabe, and M. Mori, 2017: Significant Aerosol Influence on the Recent Decadal Decrease in Tropical Cyclone Activity Over the Western North Pacific. *Geophys. Res. Lett.*, https://doi.org/10.1002/2017GL075369.

Vecchi, G. A., and B. J. Soden, 2007: Effect of remote sea surface temperature change on tropical cyclone potential intensity. *Nature*, **450**, 1066–1070, https://doi.org/10.1038/nature06423.

Villarini, G., G. A. Vecchi, T. R. Knutson, M. Zhao, and J. A. Smith, 2011: North Atlantic Tropical Storm Frequency Response to Anthropogenic Forcing: Projections and Sources of Uncertainty. *J. Clim.*, **24**, 3224–3238, https://doi.org/10.1175/2011JCLI3853.1.

Vimont, D. J., and J. P. Kossin, 2007: The Atlantic Meridional Mode and hurricane activity. *Geophys. Res. Lett.*, **34**, https://doi.org/10.1029/2007gl029683.

Wang, B., and H. Murakami, 2020: Dynamic genesis potential index for diagnosing present-day and future global tropical cyclone genesis. *Environ. Res. Lett.*, **15**, 114008, https://doi.org/10.1088/1748-9326/abbb01.

——, R. Wu, and X. Fu, 2000: Pacific-East Asian teleconnection: How does ENSO affect East Asian climate? *J. Clim.*, **13**, 1517–1536, https://doi.org/10.1175/1520-0442(2000)013<1517:PEATHD>2.0.CO;2.

——, ——, and T. I. M. Li, 2003: Atmosphere-Warm Ocean Interaction and Its Impacts on Asian-Australian Monsoon Variation*. *J. Clim.*, **16**, 1195–1211,

Accepted for publication in *Journal of Climate*. DOI 10.1175/JCLI-D-21-0529.1.

https://doi.org/10.1175/1520-0442(2003)16<1195:AOIAII>2.0.CO;2.

——, B. Xiang, and J.-Y. Lee, 2013: Subtropical High predictability establishes a promising way for monsoon and tropical storm predictions. *Proc. Natl. Acad. Sci.*, **110**, 2718–2722, https://doi.org/10.1073/pnas.1214626110.

——, and Coauthors, 2018: Towards predicting changes in the land monsoon rainfall a decade in advance. *J. Clim.*, JCLI-D-17-0521.1, https://doi.org/10.1175/JCLI-D-17-0521.1.

Wang, C., 2019: Three-ocean interactions and climate variability: a review and perspective. *Clim. Dyn.*, **53**, 5119–5136, https://doi.org/10.1007/s00382-019-04930-x.

——, and S. Lee, 2009: Co-variability of tropical cyclones in the North Atlantic and the eastern North Pacific. *Geophys. Res. Lett.*, **36**, L24702, https://doi.org/10.1029/2009GL041469.

Wang, C., and L. Wu, 2016: Interannual Shift of the Tropical Upper-Tropospheric Trough and Its Influence on Tropical Cyclone Formation over the Western North Pacific. *J. Clim.*, **29**, 4203–4211, https://doi.org/10.1175/JCLI-D-15-0653.1.

Wang, R., and L. Wu, 2013: Climate changes of Atlantic tropical cyclone formation derived from Twentieth-Century reanalysis. *J. Clim.*, **26**, 8995–9005, https://doi.org/10.1175/JCLI-D-13-00056.1.

Wang, Z., G. Zhang, T. J. Dunkerton, and F. F. Jin, 2020: Summertime stationary waves integrate tropical and extratropical impacts on tropical cyclone activity. *Proc. Natl. Acad. Sci. U. S. A.*, **117**, 22720–22726,

Accepted for publication in *Journal of Climate*. DOI 10.1175/JCLI-D-21-0529.1.

https://doi.org/10.1073/pnas.2010547117.

Wilks, D. S., 2006: *Statistical Methods in the Atmospheric Sciences*. Academic Press, 676 pp.

Wu, L., C. Wang, and B. Wang, 2015: Westward shift of western North Pacific tropical cyclogenesis. *Geophys. Res. Lett.*, **42**, 1537–1542, https://doi.org/10.1002/2015GL063450.

Wu, M., K. Yeung, and W. Chang, 2006: Trends in western North Pacific tropical cyclone intensity. *Eos, Trans. Am. Geophys. Union*, **87**, 537–538.

Wu, S., Z. Liu, R. Zhang, and T. L. Delworth, 2011: On the observed relationship between the Pacific Decadal Oscillation and the Atlantic Multi-decadal Oscillation. *J. Oceanogr.*, **67**, 27–35, https://doi.org/10.1007/s10872-011-0003-x.

Yang, Y.-M., S.-I. An, B. Wang, and J. H. Park, 2020: A global-scale multidecadal variability driven by Atlantic multidecadal oscillation. *Natl. Sci. Rev.*, **7**, 1190–1197, https://doi.org/10.1093/nsr/nwz216.

Ying, M., W. Zhang, H. Yu, X. Lu, J. Feng, Y. Fan, Y. Zhu, and D. Chen, 2014: An Overview of the China Meteorological Administration Tropical Cyclone Database. *J. Atmos. Ocean. Technol.*, **31**, 287–301, https://doi.org/10.1175/JTECH-D-12-00119.1.

Yu, J., T. Li, Z. Tan, and Z. Zhu, 2016: Effects of tropical North Atlantic SST on tropical cyclone genesis in the western North Pacific. *Clim. Dyn.*, **46**, 865–877, https://doi.org/10.1007/s00382-015-2618-x.

Yu, J. Y., P. K. Kao, H. Paek, H. H. Hsu, C. W. Hung, M. M. Lu, and S. Il An, 2015:

Accepted for publication in *Journal of Climate*. DOI 10.1175/JCLI-D-21-0529.1.

Linking emergence of the central Pacific El Niño to the Atlantic multidecadal oscillation. *J. Clim.*, **28**, 651–662, https://doi.org/10.1175/JCLI-D-14-00347.1.

Yumoto, M., and T. Matsuura, 2001: Interdecadal Variability of Tropical Cyclone Activity in the Western North Pacific. *J. Meteorol. Soc. Japan*, **79**, 23–35, https://doi.org/10.2151/jmsj.79.23.

Zhang, Q., L. Wu, and Q. Liu, 2009: Tropical Cyclone Damages in China 1983–2006. *Bull. Am. Meteorol. Soc.*, **90**, 489–496, https://doi.org/10.1175/2008BAMS2631.1.

Zhang, W., G. A. Vecchi, H. Murakami, G. Villarini, T. L. Delworth, X. Yang, and L. Jia, 2018: Dominant Role of Atlantic Multidecadal Oscillation in the Recent Decadal Changes in Western North Pacific Tropical Cyclone Activity. *Geophys. Res. Lett.*, **45**, 354–362, https://doi.org/10.1002/2017GL076397.

Zhao, J., R. Zhan, Y. Wang, and H. Xu, 2018: Contribution of the interdecadal pacific oscillation to the recent abrupt decrease in tropical cyclone genesis frequency over the Western North Pacific since 1998. *J. Clim.*, **31**, 8211–8224, https://doi.org/10.1175/JCLI-D-18-0202.1.

——, ——, ——, S. P. Xie, and Q. Wu, 2020: Untangling impacts of global warming and Interdecadal Pacific Oscillation on long-term variability of North Pacific tropical cyclone track density. *Sci. Adv.*, **6**, 1–9, https://doi.org/10.1126/sciadv.aba6813.

Figure captions:

Accepted for publication in *Journal of Climate*. DOI 10.1175/JCLI-D-21-0529.1.

Figure 1 The see-saw relationship in the TC genesis between the NA and WNP. Five-year running mean time series of (a) annual TC genesis frequency for the WNP basin (blue line) and the NA basin (red line), (b) AMO, and (c) PDO index. The blue shading represents in (a) the half standard deviation of TC genesis frequency among three datasets (CMA, JMA, and JTWC) over the WNP. Correlation coefficient R is shown in the top left of figure. The vertical grey lines roughly separate 1951-2018 into four periods with three anti-phase AMO and PDO periods (1951-1962, 1977-1998 and 1999-2018) and an in-phase of AMO and PDO period of 1963-1976.

Figure 2 Major variability region for TC genesis. Regressed TC genesis frequency anomalies (shadings, number $year^{-1}$) in each 2.5x2.5 latitude longitude box against the annual WNP TC genesis number during 1951-2018. Dots denote the regressed anomalies that are significant at a 95% confidence level. The green boxes outline the major variability regions in the WNP and the NA, respectively. The dark green contours show mean TC genesis frequency during 1951-2018.

Figure 3 Large-scale influences on the trans-basin linkage in TC genesis. Regressed July-October mean (a) vertical wind shear (shadings, m s^{-1}), (b) 850 hPa relative vorticity (shadings, 10^{-6} s^{-1}) and wind (vectors, m s^{-1}), (c) 500 hPa omega (shadings, 10^{-2} Pa s^{-1}) and SST (contours, °C), and (d) DGPI (over the WNP) and GPI (over the NA) anomalies (shadings) against the five-year running mean annual TC genesis frequency in the WNP. Green boxes outline TC major variability regions in the WNP and the NA. Dots denote the areas where regressed anomalies are significant at a 95% confidence level.

Accepted for publication in *Journal of Climate.* DOI 10.1175/JCLI-D-21-0529.1.

Figure 4 The AMO-related large-scale environment anomalies. Regressed July-October mean (a) SST (shading, °C) and wind speed (contours, m s^{-1}) and (b) 500 hPa omega (shading, 10^2 Pa s^{-1}) and 850 hPa wind (vectors, m s^{-1}) anomalies against the sign-reversed five-year running July-October mean AMO index. Contributions of each term to (d) DGPI anomalies over the WNP MVR and (e) GPI anomalies over the NA MVR. Green boxes denote TC major variability regions in the WNP and the NA. Dots (purple vectors) denote the areas where regressed SST (wind) anomalies are significant at the 95% confidence level. Total in (d) means the four terms in DGPI are varying, OM, MG, SH, and VR in (d) means DGPI for varying omega, meridional gradient of 500 hPa zonal wind, vertical wind shear, and low-level vorticity, respectively, while keeping other variables are fixed as climatology. Total in (e) means the four terms in GPI are varying. PI, RH, SH, and VR in (e) means GPI for varying potential intensity, relative humidity, vertical wind shear, and relative vorticity, respectively, while keeping other variables are fixed as climatology.

Figure 5 Atmospheric and oceanic responses to the AMO forcing. Model simulated response of (a) SST (shadings, ℃), (b) precipitation (shading, mm day^{-1}), and 850 hPa wind (vectors, m s^{-1}) (c) DGPI over the WNP and GPI over the NA (shadings) to the AMO-related SST cooling in the NA. Contours in (a) highlight the zero value of SST anomalies and the green box in (a) outlines the region where the SST is nudged to the AMO-related cooling. Green boxes in (c) denote TC major variability regions in the WNP and the NA.

Accepted for publication in *Journal of Climate*. DOI 10.1175/JCLI-D-21-0529.1.

Figures:

Accepted for publication in *Journal of Climate.* DOI 10.1175/JCLI-D-21-0529.1.

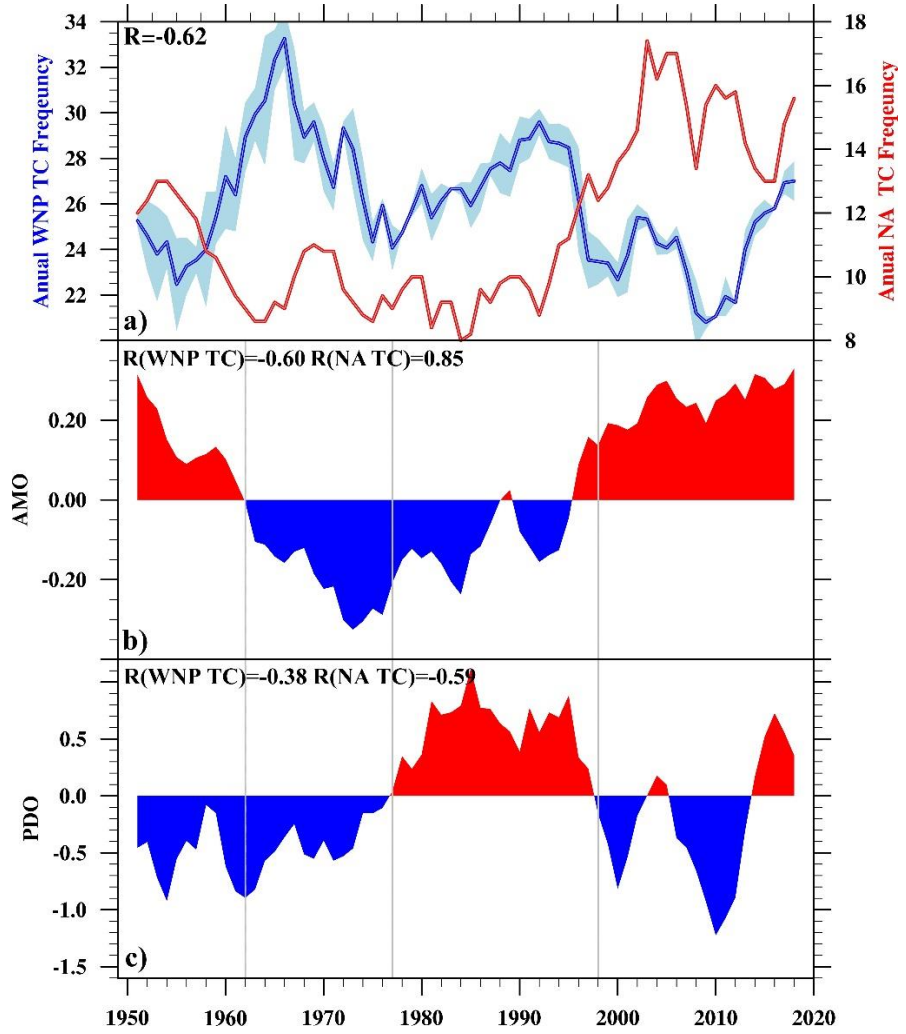

Figure 1 The see-saw relationship in the TC genesis between the NA and WNP. Five-year running mean time series of (a) annual TC genesis frequency for the WNP basin (blue line) and the NA basin (red line), (b) AMO, and (c) PDO index. The blue shading represents in (a) the half standard deviation of TC genesis frequency among three datasets (CMA, JMA, and JTWC) over the WNP. Correlation coefficient R is shown in the top left of figure. The vertical grey lines roughly separate 1951-2018 into four periods with three anti-phase AMO and PDO periods (1951-1962, 1977-1998 and 1999-2018) and an in-phase of AMO and PDO period of 1963-1976.

Accepted for publication in *Journal of Climate*. DOI 10.1175/JCLI-D-21-0529.1.

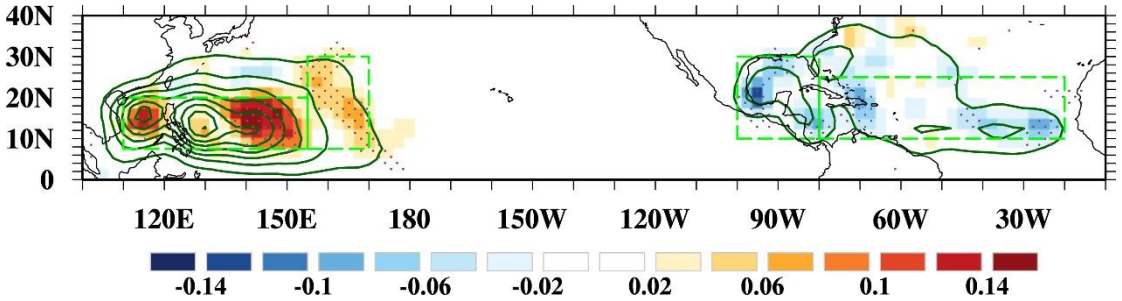

Figure 2 Major variability region for TC genesis. Regressed TC genesis frequency anomalies (shadings, number year^{-1}) in each 2.5x2.5 latitude longitude box against the annual WNP TC genesis number during 1951-2018. Dots denote the regressed anomalies that are significant at a 95% confidence level. The green boxes outline the major variability regions in the WNP and the NA, respectively. The dark green contours show mean TC genesis frequency during 1951-2018.

Accepted for publication in *Journal of Climate*. DOI 10.1175/JCLI-D-21-0529.1.

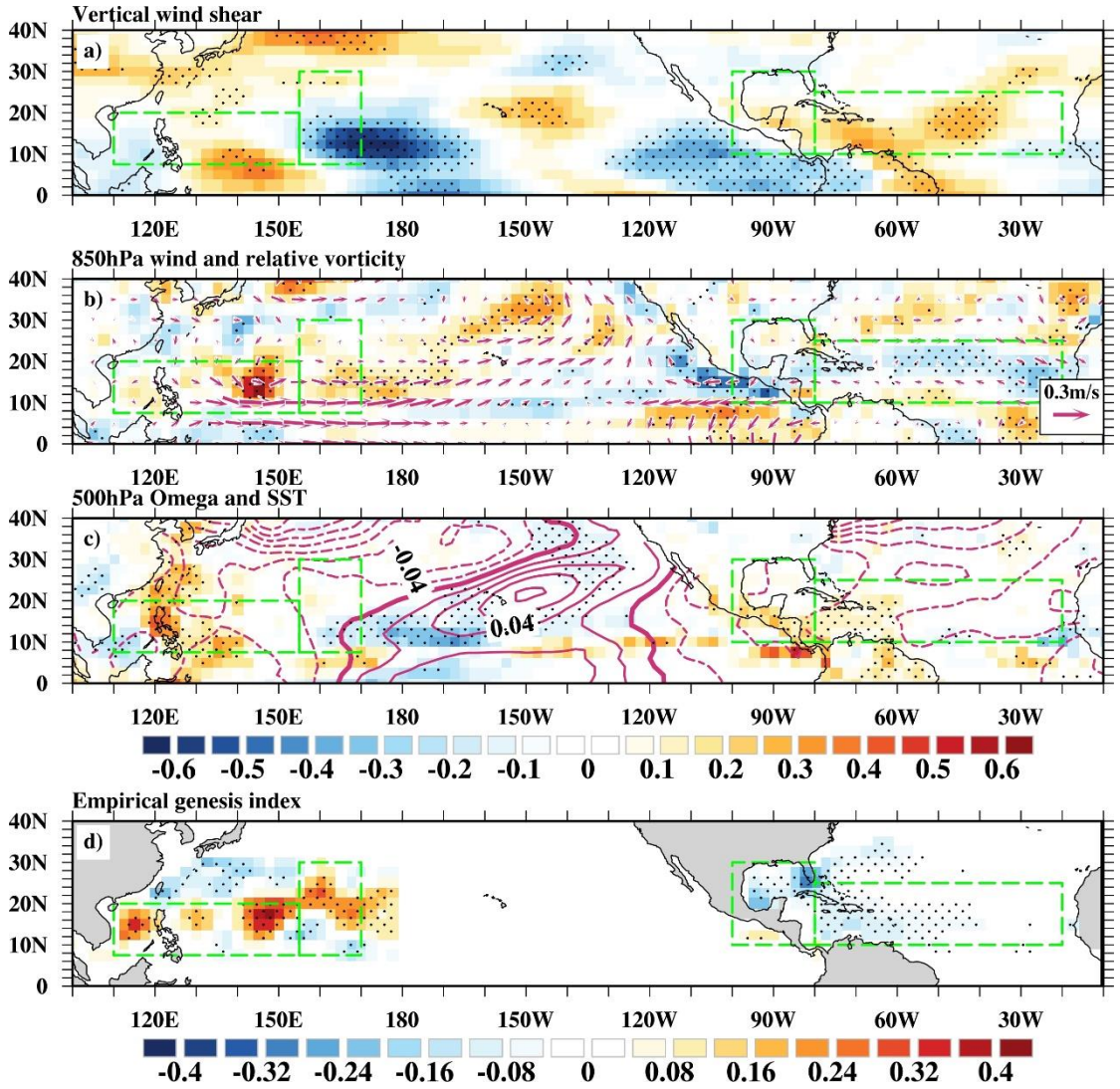

Figure 3 Large-scale influences on the trans-basin linkage in TC genesis. Regressed July-October mean (a) vertical wind shear (shadings, m s^{-1}), (b) 850 hPa relative vorticity (shadings, 10^{-6} s^{-1}) and wind (vectors, m s^{-1}), (c) 500 hPa omega (shadings, 10^{-2} Pa s^{-1}) and SST (contours, °C), and (d) DGPI (over the WNP) and GPI (over the NA) anomalies (shadings) against the five-year running mean annual TC genesis frequency in the WNP. Green boxes outline TC major variability regions in the WNP and the NA. Dots denote the areas where regressed anomalies are significant at a 95% confidence level.

Accepted for publication in *Journal of Climate*. DOI 10.1175/JCLI-D-21-0529.1.

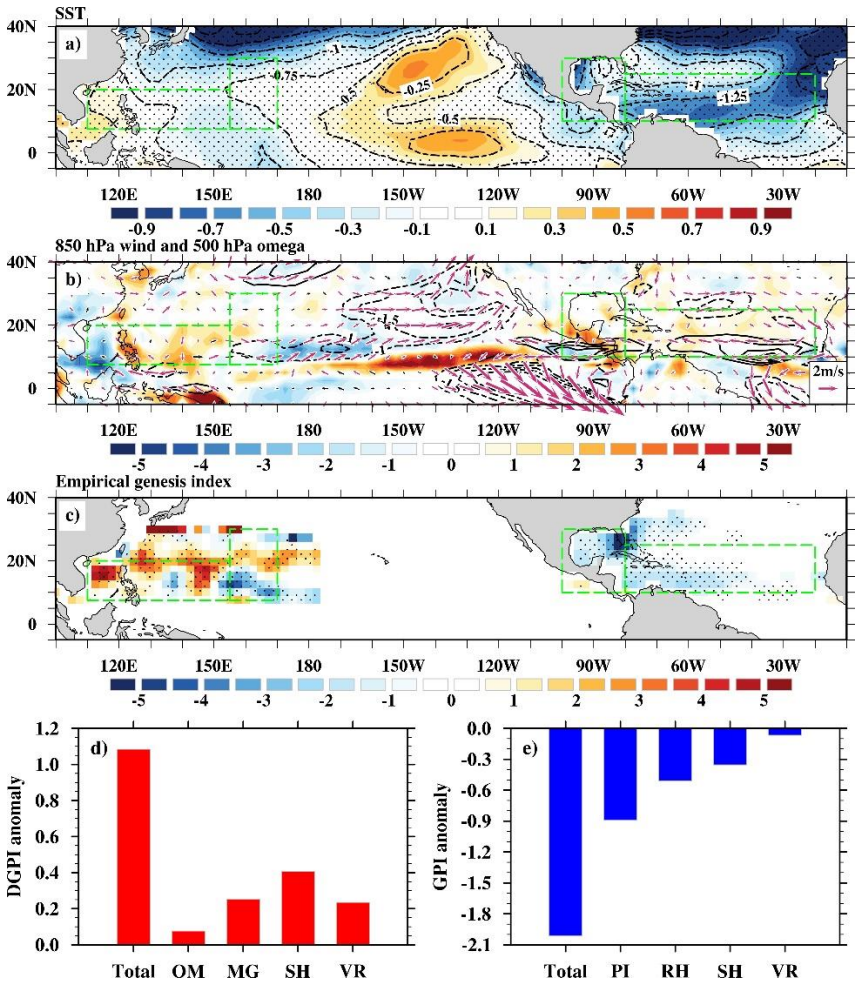

Figure 4 The AMO-related large-scale environment anomalies. Regressed July-October mean (a) SST (shading, °C) and wind speed (contours, m s^{-1}) and (b) 500 hPa omega (shading, 10^2 Pa s^{-1}) and 850 hPa wind (vectors, m s^{-1}) anomalies against the sign-reversed five-year running July-October mean AMO index. Contributions of each term to (d) DGPI anomalies over the WNP MVR and (e) GPI anomalies over the NA MVR. Green boxes denote TC major variability regions in the WNP and the NA. Dots (purple vectors) denote the areas where regressed SST (wind) anomalies are significant at the 95% confidence level. Total in (d) means the four terms in DGPI are varying, OM, MG, SH, and VR in (d) means DGPI for varying omega, meridional gradient of 500 hPa zonal wind, vertical wind shear, and low-level vorticity,

Accepted for publication in *Journal of Climate*. DOI 10.1175/JCLI-D-21-0529.1.

respectively, while keeping other variables are fixed as climatology. Total in (e) means the four terms in GPI are varying. PI, RH, SH, and VR in (e) means GPI for varying potential intensity, relative humidity, vertical wind shear, and relative vorticity, respectively, while keeping other variables are fixed as climatology.

Accepted for publication in *Journal of Climate.* DOI 10.1175/JCLI-D-21-0529.1.

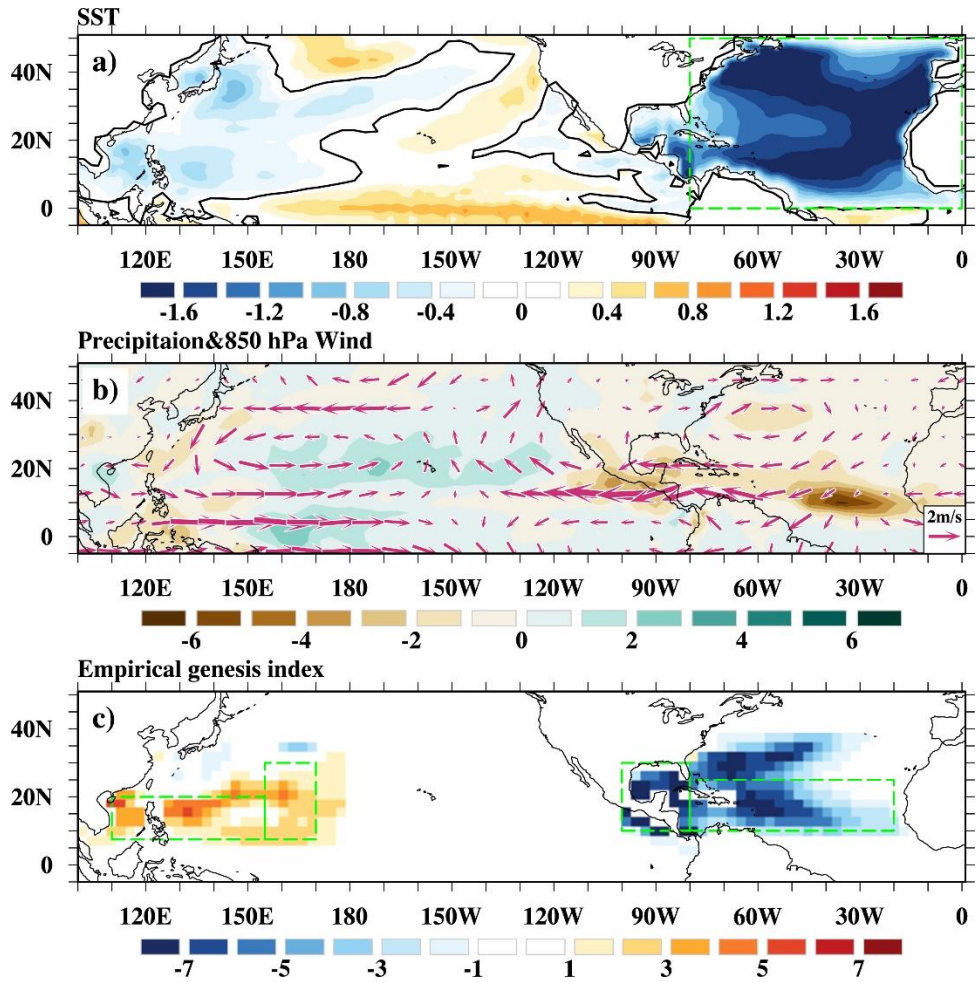

Figure 5 Atmospheric and oceanic responses to the AMO forcing. Model simulated response of (a) SST (shadings, ℃), (b) precipitation (shading, mm day^{-1}), and 850 hPa wind (vectors, m s^{-1}) (c) DGPI over the WNP and GPI over the NA (shadings) to the AMO-related SST cooling in the NA. Contours in (a) highlight the zero value of SST anomalies and the green box in (a) outlines the region where the SST is nudged to the AMO-related cooling. Green boxes in (c) denote TC major variability regions in the WNP and the NA.

Accepted for publication in *Journal of Climate*. DOI 10.1175/JCLI-D-21-0529.1.